Chapter 4

SCINTILLATION TECHNIQUE FOR PROBING IONOSPHERIC IRREGULARITIES

Santimay Basu
Geophysics Laboratory (LIS)
Hanscom AFB, MA 01731

Sunanda Basu
Physics Research Division
Emmanuel College
Boston, MA 02115

ABSTRACT

The phenomenon of radio wave scintillation caused by ionospheric irregularities of electron density are described. The different indices of scintillation that provide a measure of intensity and phase scintillation have been defined. Both simple and sophisticated receiving systems used for recording scintillations are briefly described. The use of scintillation experiments in exploring the physical mechanisms of irregularity formation and in defining the constraints of practical communication systems are outlined.

INTRODUCTION

Radio waves from satellites or radio stars during their passage through the ionospheric irregularities of electron density develop random phase fluctuations across the wavefront. As the wavefront travels towards the ground, phase mixing occurs and, as a result, not only phase but amplitude fluctuations as well, develop on the ground. Due to the relative motion between the satellite, the ionosphere and the receiver on ground, the spatial pattern of amplitude and phase variation sweeps past the receiver and temporal variations of phase and amplitude known as scintillations are recorded by the receiver. In the case of radio stars or geostationary satellites, the temporal variation is caused by the ionospheric drift whereas in the case of low altitude (≈1000 km) orbiting satellites, the satellite motion projected on to the ionosphere dictates the temporal structure.

SCINTILLATION PARAMETERS

The amplitude and phase fluctuations of the recorded signal are statistically characterized by two major parameters, amplitude and phase scintillation indices, denoted respectively by S_4 and σ_ϕ. Additional parameters such as the signal decorrelation time and spectral shape of signal fluctuations are also of importance for specifying effects on systems.

Scintillation Index, S_4

The amplitude scintillation index, S_4, is defined as the ratio of the standard deviation of signal intensity and the average signal intensity and defined as

$$S_4 = \frac{(<I^2> - <I>^2)}{<I>^2} \qquad (1)$$

The time interval over which this parameter is computed depends on the time period over which the signal fluctuations are observed to be stationary. For geostationary satellite

observations, a 3-minute to 15-minute data segment has been considered to be optimum whereas for orbiting satellites a data segment varying between 10-30 seconds has been used.

RMS Phase Deviation, σ_ϕ

The phase scintillation index is defined as the standard deviation of a linearly detrended phase data segment. The linear detrending over the appropriate data segment discussed in the previous paragraph removes the background phase variation caused by smooth changes of ionization density. Thus the phase scintillation index is defined as

$$\sigma_\phi = (<\phi^2> - <\phi>^2)^{1/2} \tag{2}$$

Intensity Decorrelation Time, τ_I

In addition to the above two parameters the intensity decorrelation time, τ_I, defined as the time shift required to obtain signal correlation of 0.5 is also important. The decorrelation time, τ_I, is defined as

$$\frac{<I(t)\, I(t+\tau_I)>}{<I(t)>^2} = 0.5 \tag{3}$$

In the case of receiving systems capable of acquiring both signal amplitude and phase from a satellite source, the complex decorrelation time can be obtained by replacing the intensity terms in Eq. (3) by the complex amplitude.

Scintillation Spectrum

The time series of intensity and phase scintillation can be analyzed by the standard Fast Fourier Transform (FFT) or Maximum Entropy Method (MEM) to derive a plot of the variation of the power spectral density of amplitude or phase as a function of fluctuation frequency. The length of the data sample chosen for such spectral analysis needs to be stationary. For geostationary satellite observations a 3-minute scintillation data sample is, in general, found to be optimum. In such applications, the data digitization rate is required to be in the range of 30-50 Hz. The frequency range of the spectral analysis is dictated at the low frequency end by the inverse of the data sample duration and at the high frequency end by the Nyquist frequency which is half of the digitization rate. Thus for a 180-sec data segment from a geostationary satellite and 50-Hz sampling frequency, the frequency interval over which the spectrum is obtained corresponds to .0056 Hz to 25 Hz. For an average ionospheric drift of 50 ms^{-1}, the above frequency interval corresponds to spatial irregularity wavelength range of 8.9 km to 2 m. In the equatorial region, when strong to moderate levels of scintillations are observed, the ionospheric drift typically varies smoothly between 200 ms^{-1} to 50 ms^{-1} in the course of an evening which changes the coverage of irregularity wavelengths by a factor of 4. At high latitudes, the ionospheric drift variations are more severe with drifts changing from 50 ms^{-1} to 2000 ms^{-1} in a matter of minutes. Thus the irregularity wavelengths covered by the spectral analysis can vary greatly at high latitudes.

For orbiting satellites, at an altitude of 1000 km, the scan velocity of the propagation path through the F-region height of 300 km corresponds to 2.2 km/sec. The temporal structure of scintillation is, therefore, dictated by the scan velocity except at high latitudes where the ionospheric drift may not, on occasions, be negligible. In the case of orbiting satellites, data length of 10 sec and digitization rate of 125 Hz is found to be optimum. Considering only the ionospheric scan velocity, the above parameters provide an irregularity wavelength coverage of 22 km to 18 m.

The scintillation parameters, defined above, can be readily computed from digital recordings. Many scintillation recording systems still employ chart recorders instead of digital recorders. For such systems, Whitney et al. [1969] defined the amplitude scintillation magnitude, SI_{dB}, in terms of dB excursions between the third peak up from the minimum and third peak down from the maximum signal levels. By providing calibrations with a signal source applied to the antenna input terminals of the receiver in terms of dB and using relatively fast chart speed so that the individual fadings and signal enhancements can be delineated, the third peak method is a useful way to quantify the analog recordings. Comparing digital and analog recordings Whitney et al. [1969] showed that the third peak method provides the dB excursions between the 2nd and 98th percentiles of signal fluctuations. In addition, he provided a useful graph that can be used to convert SI (dB) indices to S_4 indices. Attempts have also been made to manually digitize fast chart recordings to derive scintillation spectra. Reliability of such spectra is, however, limited because the response time of chart recorders does not exceed a few Hz thereby limiting the Nyquist frequency to 1 Hz or less. Since strong scintillations often contain fluctuation frequencies that exceed 10 Hz, manually derived spectra often provides misleading results.

SCINTILLATION RECORDING SYSTEMS

Total Power Recording System

The total power or systems recording intensity scintillations from geostationary satellites transmitting circularly polarized signals in the VHF range (typically at 136, 137, 244 and 257 MHz) can be achieved by a simple system. It consists of a ten element Yagi antenna, a commercial converter (noise figure of 3 dB, conversion gain of 10 dB) that converts VHF frequencies to a radio frequency (typically 28 MHz or 10.7 MHz) followed by a communications receiver tuned to accept the converted frequency, and operated with an IF bandwidth of 4 or 8 KHz. The above IF bandwidth is found to be wide enough to be unaffected by the frequency drift of the local oscillator. The communication receiver is operated in the fast AGC mode providing a time constant of .01 sec. The AGC voltage is fed to a chart recorder. In order to protect the pen from jitter, an external RC circuit with a time constant of 0.1 to .05 sec is often inserted between the AGC port and the pen recorder. The pen recorder is usually equipped with a d.c. buckout facility. The signals from geostationary satellites received with a ten-element Yagi antenna usually develop 110 dBm at the converter input. In order to calibrate the system, the antenna is disconnected from the converter and a calibrating signal source (providing 100-120 dBm at VHF followed by attenuators capable of varying the attenuation over a 100-dB range in 1-dB steps) is connected to the converter input. This is used to obtain calibration levels in the chart recorder at 1 to 3-dB intervals over the full scale deflection range. The system is so adjusted that the satellite signal level runs at a level 6 dB below the full-scale deflection. It should be noted that for scintillations arising from a diffraction process, the positive excursions do not exceed a 6-dB level although the associated negative excursions may approach 25 dB.

Recording of amplitude scintillations of L-band signals from stationary satellites can be achieved with a similar system by replacing the Yagi antenna with an 8-ft paraboloidal antenna and a low noise L-band converter.

With the advent of desktop computers, the AGC signal after d.c. buckout can be digitally recorded on a disk and processed to obtain the full range of statistical parameters, such as, S_4 index, decorrelation time , and scintillation spectrum, on a real-time basis.

Phase and Amplitude Scintillation Recording from Stationary Satellites

Stationary satellites transmitting single frequency phase coherent signals have been used to record both amplitude and phase scintillations by using a sophisticated computer-controlled receiver.

For such measurements an extended dynamic range receiver with an extremely stable local oscillator is employed. The receiver operates under computer control and once tuned to within a few hertz of a signal detected in a 10-Hz bandwidth, self-tunes to within ±1 millihertz of the mean frequency as determined by the zero crossings averaged over a 20-sec period. Subsequent changes in frequency, either due to changes in ionospheric or geometrical doppler, are sensed by the system, which then retunes. At each retune, the local oscillator frequency information is recorded to allow reconstruction of the long-term phase in subsequent processing. In this way the system can measure signal phase variations with precision as would a coherent system except for any long-term relative frequency drifts between the satellite and receiver references.

Once a signal is properly acquired by the receiver, its quadrature components are sampled at 10 Hz and are digitally recorded along with time and pertinent system information. During initial off-line processing, these data are converted to signal intensity and continuous phase. While simple in concept the generation of continuous phase over long observation periods is prone to numerical difficulties. Since this is a single frequency measurement, the accumulation of phase over a period of several hours can result in extremely large values. These problems have been avoided by calculation and removal of the largest scale (for example, few hours) dispersive doppler changes during pre-processing.

Following initial processing, only phase variations with periods shorter than some tens of minutes remain. The data can then be treated using methods similar to those designed for, and proven, during the Wideband experiment [Fremouw et al., 1978]. Basically, this consists of separation of rapidly varying scintillation components of the signal from the longer term trends. The spectral components are separated by passing the phase data through a sharp cutoff high pass digital filter (f_c = 0.0067 Hz); there is generally no need to filter signal intensity, which has no low frequency component in the constant signal level, geostationary case.

PHASE AND AMPLITUDE SCINTILLATION MEASUREMENTS WITH MULTIFREQUENCY BEACON TRANSMISSIONS

DNA Wideband Satellite

Complex signal scintillation measurements have been performed by using multifrequency coherent radio beacon transmissions from an orbiting satellite. In 1976, the U.S. Defense Nuclear Agency launched the DNA Wideband satellite in a 1000-km orbit which radiated ten coherent radio spectral lines between the VHF and S bands [Fremouw et al., 1978]. The ten spectral lines were derived from a fundamental frequency of 11.4729 MHz and corresponded to one VHF, seven UHF, one L-band and one S-band transmission. The receiving system consisted of a tracking antenna and a receiver which was designed to maintain the coherence of the transmitted signals. The receiver incorporated a frequency synthesizer which generated a replica of the transmitted signal spectrum which were offset by the intermediate frequencies to generate the local oscillator signals.

The synthesizer was phase-locked by a loop operating on the output of the S-band reference receiver. Except for the first mixer, the reference receiver was identical to the measurement receiver channels at various frequencies. Nine measurement receiver channels were employed; one for VHF , one each for seven UHF channels, and one for L band. Remote receiving antennas comprised of identical measurement channels were used to perform spaced receiver scintillation observations.

The signals in each receiver channel were finally translated to an essentially zero frequency baseband by means of two quadrature detectors. The receiving system thus provided coherently detected in-phase and quadrature components at VHF, seven UHF, and one L-band channel. Thus

phase and intensity scintillation indices at all these frequencies, as well as, the second order statistics of complex signal scintillation in the temporal, spatial and spectral domains could be obtained. In addition to scintillation measurements, the second difference of phase measurement at the three UHF comb frequencies provided the total electron content (TEC) of the ionosphere.

The second difference of phase, $\Delta_2\phi$, is obtained by first forming the phase difference between a carrier and its upper sideband (413 MHz and 435 MHz) and the same carrier and its lower sideband (390 MHz and 413 MHz) and then taking the difference of the two differences. It can be shown [Fremouw et al., 1978] that

$$\Delta_2\phi = \frac{e^2}{2\pi\varepsilon_o m c}\frac{f_m^2}{f^3} N_T$$

where, e - electronic charge,
m - mass of an electron,
ε_o - permittivity of free space,
c - speed of light,
f_m - the frequency separation between the UHF triad,
f - center UHF frequency of the triad,
N_T - total electron content up to satellite height.

The full complement of Wideband satellite signals were monitored from the auroral location of Poker Flat, Alaska, and the equatorial locations of Ancon, Peru and Kwajalein, Marshall Island. A brief period of Wideband satellite measurement was initially performed at Stanford, California through the relatively undisturbed ionosphere. The satellite was placed in a sun-synchronous orbit so that equatorward crossings were obtained around 1120 and 2320 local time and the auroral ionosphere was intercepted in the post-midnight time frame. The nighttime equator crossings could have been a couple of hours earlier for the interception of most intense early evening irregularities.

DNA HiLat Satellite

The DNA HiLat satellite was launched on June 27, 1983 in a near circular 800-km orbit with an inclination of 82°. The satellite carried a beacon transmitter package similar to the Wideband satellite, but, in addition, performed satellite in-situ measurements which were telemetered to ground using the L-band transmission of the beacon. The objective of the mission was to characterize the physical environment of the upper atmosphere through in-situ measurements, establish their relationship with the generation of plasma density irregularities and measure the effects of the irregularities on radio wave propagation. The beacon transmitter provided coherent transmission at L-band (1239 MHz), three UHF frequencies (447, 413 and 378 MHz), and one at VHF (138 MHz). The L-band signal while serving as a phase reference for phase scintillation measurement was also modulated by the telemetry signal. At the receiver, an L-band carrier recovery loop has been used to generate the reference signal for the demodulation of the telemetry data and synchronous demodulation of the UHF and VHF frequencies.

The HiLat satellite in-situ instrument package consisted of a J-sensor for the measurement of the local flux of electrons over the energy range of 20 eV to 20 keV in 16 channels, a magnetometer for the measurement of field-aligned 'Birkeland' currents, an ion drift meter for the measurement of thermal ion density and cross track ion drift, a retarding potential analyzer for the measurement of the ram component of ion drift, ion composition and ion temperature and an electron Langmuir probe. In addition, a vacuum ultraviolet (UV) imager was included to obtain auroral UV images in full daylight in selectable spectral windows over the range of 1100 Å to 2078 Å. The in-situ package provided an excellent array of instruments that characterized the

currents, particles and fields in the high latitude ionosphere.

The data from the HiLat satellite were acquired at Sondrestrom, Greenland located in the dayside cusp region and at Fort Churchill,.Canada and Tromso, Norway corresponding to two auroral locations in the American and European sectors. In addition, a portable Rover receiving system normally located at Bellevue, Washington could be deployed anywhere at high latitudes to perform campaign observations.

The Polar Bear Satellite

This satellite carrying a beacon package identical to that of the HiLat satellite but more limited in-situ instrumentation providing UV imaging and magnetometer measurements only was launched in 1986. Both HiLat and Polar Bear satellites were monitored with identical receiving systems at the four high latitude locations mentioned above.

APPLICATION OF SCINTILLATION MEASUREMENTS

Scintillation measurements have been used as a key diagnostic for the presence of the irregularities of electron density in the ionosphere. This knowledge is important, on one hand, to determine the spatial and temporal distribution of the ionospheric irregularities and to understand the physical processes that lead to the formation of such irregularities. On the other hand, the characteristics of the scintillating signal structure determines how the performance of a communication link or a radar system can be degraded. The key scintillation characteristics that contribute to our knowledge of geophysics and the parameters that dictate the degradation of system performance are briefly summarized in the following paragraphs.

The key irregularity parameter, namely the integrated electron density deviation (ΔN) of the ionospheric irregularities, can be derived from intensity and phase scintillation measurements. In the framework of weak scatter theory the intensity and phase scintillation indices, S_4 and σ_ϕ, have been related [Rino, 1979] to ΔN and the geometrical term accounting for both the geometry of the propagation path and the irregularity anisotropy. Of the two scintillation indices, the phase scintillation index, σ_ϕ, is more useful as it is related, in a straightforward manner, to the irregularity parameters.

The other irregularity parameter of great importance to our understanding of the generation of irregularities is related to the form and shape of the irregularity spectrum. The scintillation spectrum reflects the form of the irregularity spectrum and the spectral index of scintillation has been simply related to the 3-dimensional irregularity spectral index. As such, the spectral studies of both intensity and phase scintillations have been performed and important conclusions regarding the irregularity spectral shapes, spectral indices and drifts have been derived [Basu et al., 1985].

Scintillation measurements, because of their relative simplicity, have been most useful in determining global morphology of irregularities. Earlier reviews were presented by Aarons [1982] and Yeh and Liu [1982]. Figure 1 taken from S. Basu et al. [1988] provides a synopsis of the global distribution of scintillation occurring regions during the solar maximum and minimum periods.

Since the maximum scintillation amplitude occurs in the equatorial region, specialized reviews have appeared which deal only with this region [Aarons, 1977; Basu and Basu, 1981; 1985]. The latter two reviews discuss the impact of equatorial plasma density depletions or "bubbles" caused by the Rayleigh Taylor instability [Ossakow, 1981] on scintillation magnitude and longitudinal variability in this region. Further, data from the equatorial anomaly region have been used to study the effects of scintillations on communications and radar systems through the variability of spectral

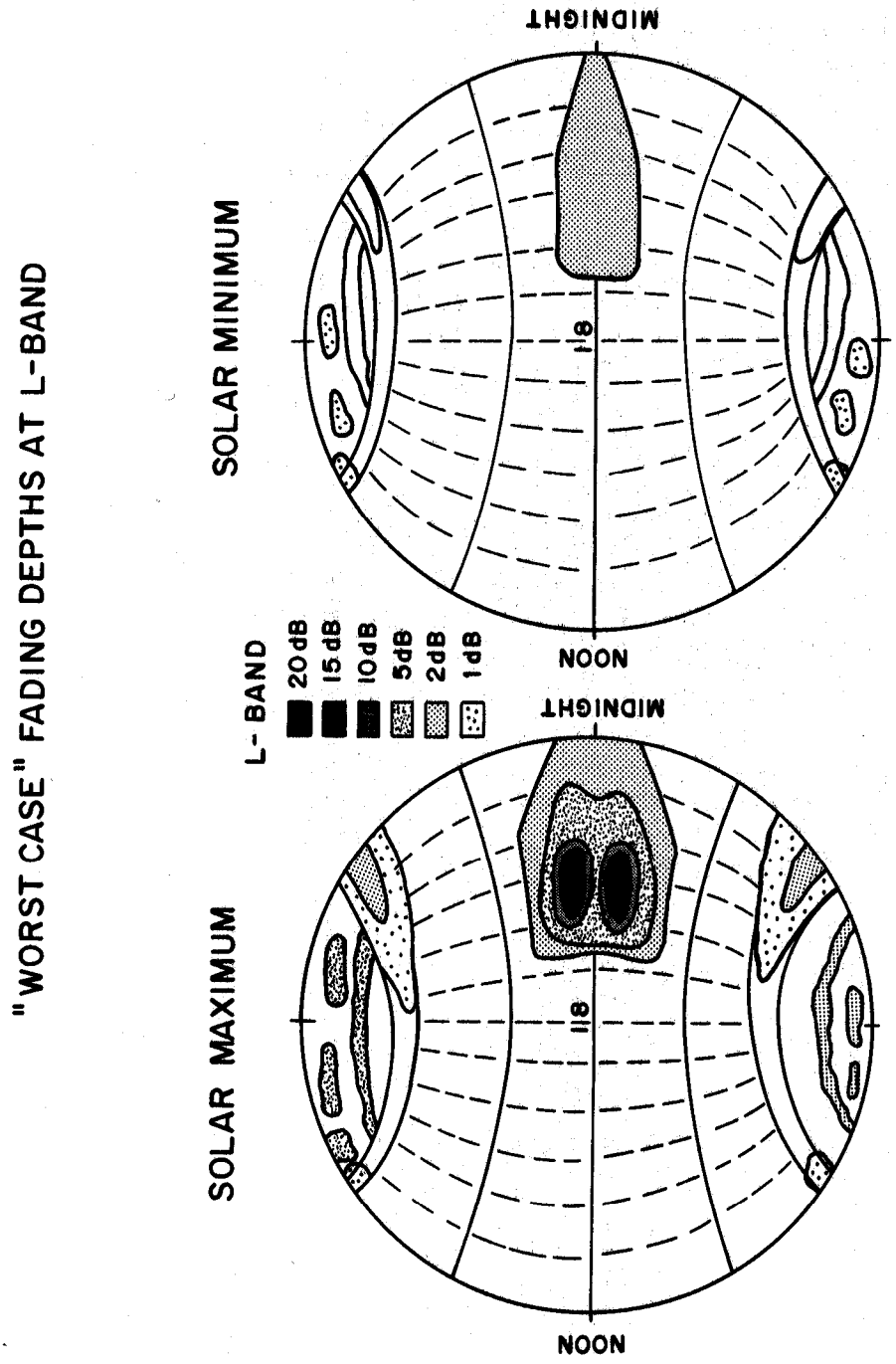

Figure 1. Global variation of scintillation fades during solar maximum and solar minimum.

shape, decorrelation time, cumulative distribution functions of signal amplitude, fade durations, the distribution of phase and intensity rates, and depolarization effects caused by diffractive scattering [Su. Basu et al., 1983; S. Basu et al., 1987; Lee et al., 1982; Franke and Liu, 1983].

At high latitudes the scintillation technique was the first to establish that the polar cap was the seat of large amplitude irregularities during solar maximum [Aarons et al.., 1981; Su. Basu et al., 1985] which could be caused by the gradient-drift instability occurring at the edges of convecting plasma density enhancements known as patches [Weber et al., 1984; Tsunoda, 1988] or by F-layer sun-aligned arcs [Weber and Buchau, 1981]. The DNA Wideband satellite did much to elucidate the sheet-like anisotropy of auroral irregularities and their morphology [Fremouw et al., 1977; Rino et al., 1978; Rino and Matthews, 1980], while the DNA HiLat satellite with its complement of scintillations and in-situ package was instrumental in identifying velocity shears as a viable source of small-scale irregularities in the ionosphere [Su. Basu et al., 1986].

Thus we find that scintillation measurements, particularly in conjunction with other diagnostics, have contributed greatly to our understanding of plasma processes in the coupled magnetosphere-ionosphere-thermosphere system. Multi-frequency scintillation studies have provided guidelines for the design of communication systems.

ACKNOWLEDGEMENT

The work at Emmanuel College was supported by AFGL Contract F19628-86-K-0038.

REFERENCES

Aarons, J., Equatorial scintillations: A review, IEEE Trans. Antennas Propagat., AP-25, 729, 1977.

Aarons, J., Global morphology of ionospheric scintillations, Proc. IEEE, 70, 360, 1982.

Aarons, J., J.P. Mullen, H.E. Whitney, A. Johnson, and E. Weber, VHF scintillation activity over polar latitudes, Geophys. Res. Lett., 8, 277, 1981.

Basu, S. and Su. Basu, Equatorial scintillations - a review, J. Atmos. Terr. Phys., 43, 473, 1981.

Basu, Su. and S. Basu, Equatorial scintillations: Advances since ISEA-6, J. Atmos. Terr. Phys., 47, 753, 1985.

Basu, S., E.M. MacKenzie, Su. Basu, E. Costa, P.F. Fougere, H.C. Carlson, Jr., and H.E. Whitney, 250 MHz/GHz scintillation parameters in the equatorial, polar and auroral environments, IEEE J. Selec. Areas Commun., SAC-5, 102, 1987.

Basu, S., E. MacKenzie, and Su. Basu, Ionospheric constraints on VHF/UHF communications links during solar maximum and minimum periods, Radio Sci., 363, 1988.

Basu, Su., S. Basu, J.P. McClure, W.B. Hanson, and H.E. Whitney, High-resolution topside in-situ data of electron densities and VHF/GHz scintillations in the equatorial region, J. Geophys. Res., 88, 403, 1983.

Basu, Su., S. Basu, E. MacKenzie, and H.E. Whitney, Morphology of phase and intensity scintillations in the auroral oval and polar cap, Radio Sci., 20, 347, 1985.

Basu, Su., S. Basu, C. Senior, D. Weimer, E. Nielsen, and P.F. Fougere, Velocity shears and sub-km scale irregularities in the nighttime auroral F-region, Geophys. Res. Lett., 13, 101, 1986.

Franke, S.J. and C.H. Liu, Observations and modeling of multi-frequency VHF and GHz scintillations in the equatorial region, J. Geophys. Res., 88,. 7075, 1983.

Fremouw, E.J., C.L. Rino, R.C. Livingston, and M.D. Cousins, A persistent subauroral scintillation enhancement observed in Alaska, Geophys. Res. Lett., 4, 539, 1977.

Fremouw, E.J., R.L. Leadabrand, R.C. Livingston, M.D. Cousins, C.L. Rino, B.C. Fair, and R.A. Long, Early results from the DNA Wideband satellite experiment - complex-signal scintillation, Radio Sci., 13, 167, 1978.

Lee, M.C., A. DasGupta, J.A. Klobuchar, S. Basu, and Su. Basu, Depolarization of VHF geostationary satellite signals near the equatorial anomaly crest, Radio Sci., 17, 399, 1982.

Ossakow, S.L., Spread-F theories - a review, J. Atmos. Terr. Phys., 43, 437, 1981.

Rino, C.L., A power-law phase screen model for ionospheric scintillation, 1, Weak scatter, Radio Sci., 14, 1135, 1979.

Rino, C.L. and S.J. Matthews, On the morphology of auroral zone radio wave scintillation, J. Geophys. Res., 85, 4139, 1980.

Rino, C.L., R.C. Livingston, and S.J. Matthews, Evidence for sheet-like auroral ionospheric irregularities, Geophys. Res. Lett., 5, 1039, 1978.

Tsunoda, R.T., High-latitude F-region irregularities: a review and synthesis, Revs. Geophysics, 26, 719, 1988.

Weber, E.J. and J. Buchau, Polar cap F layer auroras, Geophys. Res. Lett., 8, 125, 1981.

Weber, E.J., J. Buchau, J.G. Moore, J.R. Sharber, R.C. Livingston, J.D. Winningham, and B.W. Reinisch, F layer ionization patches in the polar cap, J. Geophys. Res., 89, 1683, 1984.

Whitney, H.E., J. Aarons, and C. Malik, A. proposed index for measuring ionospheric scintillations, Planet. Space Sci., 17, 1069, 1969.

Yeh, K.C. and C.H. Liu, Radiowave scintillations in the ionosphere, Proc. IEEE, 70, 324, 1982.